Identification of Oxidation-Sensitive Peptides within the Cytoplasmic Domain of the Sarcoplasmic Reticulum Ca^{2+}-ATPase†

Rosa I. Viner,‡ Arkadi G. Krainev,§ Todd D. Williams,|| Christian Schöneich,‡ and Diana J. Bigelow*,§

Departments of Biochemistry and Pharmaceutical Chemistry and Mass Spectrometry Laboratory, The University of Kansas, Lawrence, Kansas 66045

Received January 10, 1997; Revised Manuscript Received April 15, 1997⊗

ABSTRACT: We have examined the oxidative sensitivity of the Ca^{2+}-ATPase of skeletal muscle sarcoplasmic reticulum (SR) membranes, exposing isolated SR membranes to the thermolabile water soluble free radical initiator, 2,2′-azobis(2-amidinopropane) dihydrochloride (AAPH). Incubation with up to 702 μM AAPH-derived radicals results in a concentration- and time-dependent inhibition of calcium-dependent ATPase activity correlating with the loss of monomeric Ca^{2+}-ATPase polypeptides, and the concomitant appearance of higher molecular weight species. However, no oxidant-induced protein fragmentation is detected. The observed formation of oxidant-induced bityrosine accounts for the intermolecular Ca^{2+}-ATPase cross-links, as well as intramolecular cross-links. The oxidation of sulfhydryl groups to disulfides as another possible source of intermolecular cross-links has been ruled out after examination of SDS−PAGE performed under both reducing and non-reducing conditions. Exposure of the SR membranes to AAPH-derived radical species results in a small degree of lipid peroxidation that is not correlated with enzyme inactivation, suggesting that modification of membrane-spanning peptides is not related to enzyme inactivation. Six cytoplasmic peptides have been identified that are modified by exposure to AAPH or, alternatively, to hydrogen peroxide, suggesting that these regions of the Ca^{2+}-ATPase are generally sensitive to oxidants. These oxidized peptides were identified after separation by reversed-phase HPLC followed by N-terminal sequencing and amino acid analysis as corresponding to the following sequences of the Ca^{2+}-ATPase: (i) Glu_{121} to Lys_{128}, (ii) His_{190} to Lys_{218}, (iii) Asn_{330} to Lys_{352}, (iv) Gly_{432} to Lys_{436}, (v) Glu_{551} to Arg_{604}, and (vi) Glu_{657} to Arg_{671}. The Glu_{551} to Arg_{604} peptide, located within the nucleotide binding domain, was found to participate in the formation of intermolecular bityrosine cross-links with the identical Glu_{551} to Arg_{604} peptide from a neighboring Ca^{2+}-ATPase polypeptide chain.

Reactive oxygen metabolites have been implicated in a variety of pathophysiological conditions including atherosclerosis, post-ischemic tissue injury, arthritis, cancer, Parkinson's disease, and other age-related dysfunctions (*1*−*3*). In addition, oxy radicals have been suggested to play an important role in mediating the tissue injury associated with the metabolism of certain drugs and xenobiotics (*4, 5*). An early event associated with oxidative stress is the loss of calcium homeostasis (*6*). The Ca^{2+}-ATPase of sarcoplasmic or endoplasmic reticulum is the major active calcium transport protein responsible for the maintenance of normal intracellular calcium levels in a variety of cell types. Hence the potential oxidative damage of these Ca^{2+}-ATPases by reactive oxygen species may contribute to the increased levels of intracellular calcium that lead to cellular damage. Indeed, defects in this enzyme have been seen to accompany oxidative stress in several instances. For example, ischemia/reperfusion injury in the heart has been shown to involve oxidant-mediated damage to the cardiac isoform of the Ca^{2+}-ATPase (*7*). Furthermore, aging that is hypothesized to result from chronic but mild oxidative stress is associated with dysfunction of the skeletal muscle Ca^{2+}-ATPase (*8*−*10*).

However, the underlying mechanism of these defects has not been defined. Therefore we have explored the effects of oxidation on active calcium transport utilizing sarcoplasmic reticulum (SR)[1] membranes from fast twitch skeletal muscle as an abundant source of the Ca^{2+}-ATPase. The present study reports the detailed molecular characterization of the free radical-induced modification of the SR Ca^{2+}-ATPase correlated with its functional properties. These studies serve as a model for rationalizing the loss of calcium homeostasis under conditions of oxidative stress *in vivo* on a molecular level. For this purpose, we have chosen to expose SR membranes to oxygen-centered free radicals, generated in a controlled chemical reaction by employing the thermolabile, water-soluble free radical initiator 2,2′-azobis(2-amidinopropane) dihydrochloride (AAPH). In the

† This work was supported by the National Institute of Aging, Grants RO1 AG12275 and PO1 AG12993. The tandem mass spectrometer was purchased with the aid of a National Institutes of Health Grant S10 RRO 6294-01 (T.D.W.) and the University of Kansas. This work was further supported by grants from the Scientific Education Partnership, a Marion Merrell Dow Foundation; the Research Development Fund of the University of Kansas; the American Federation for Aging Research; and the Association for International Cancer Research.

* To whom correspondence should be addressed at The University of Kansas, Department of Biochemistry, Haworth Hall 5060, Lawrence, KS 66045-2106. Phone: (913) 864-3831. FAX: (913) 864-5321.

‡ Department of Pharmaceutical Chemistry.

§ Department of Biochemistry.

|| Mass Spectrometry Laboratory.

⊗ Abstract published in *Advance ACS Abstracts,* June 1, 1997.

[1] Abbreviations: AAPH, 2,2′-azobis(2-amidinopropane) dihydrochloride; BSA, bovine serum albumin; DNPH, 2,4-dinitrophenylhydrazone; DTNB, 5,5′-dithiobis(2-nitrobenzoic acid); cfFAB, continuous flow fast atom bombardment; GSH, glutathione (reduced form); HPLC, high-performance liquid chromatography; MOPS, 3-(*N*-morpholino)-propanesulfonic acid; MS, mass spectrometry; SDS−PAGE, sodium dodecyl sulfate polyacrylamide gel electrophoresis; SR, sarcoplasmic reticulum; t_R, retention time.

S0006-2960(97)00058-5 CCC: $14.00

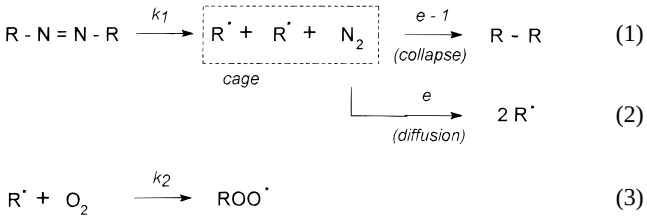

FIGURE 1: Reaction scheme for the thermolytic cleavage of AAPH.

presence of molecular oxygen the latter selectively forms peroxyl radicals via reactions 1 through 3 (Figure 1; *11*).

The rate of free radical initiation (R_i) is described by eq 4, where *e* is the efficiency of the free radical R• escape from the cage, permits the calculation of the total amount of AAPH-generated radical under defined experimental conditions.

$$R_i = 2ek_1[\text{R—N═N—R}] \quad (4)$$

Due to the low value of R_i [1.36×10^{-6} s^{-1} at 37 °C (*12*)] and a near-diffusion-controlled value of k_2 (ca. 10^9 M^{-1} s^{-1}), a constant rate of peroxyl radical (ROO•) formation may be obtained when using relatively large initial amounts of AAPH, i.e., 10−100 mM. Peroxyl radicals can induce peroxidation of biomolecules and have been shown to be significantly involved in lipid and protein radical chain oxidations under conditions of oxidative stress (*2, 13*). In addition, peroxyl radicals can recombine (reaction 5) to produce alkoxyl radicals (RO•).

$$\text{ROO}^\bullet + \text{ROO}^\bullet \xrightarrow{k_3} \text{RO}^\bullet + \text{RO}^\bullet + \text{O}_2 \quad (5)$$

The presence of alkoxyl radicals must also be considered, based on our previous spin trapping and direct ESR measurements demonstrating that these radicals can be formed by AAPH in aqueous solutions (*14, 15*).

Although other pathways such as metal-catalyzed oxidation may be equally important under conditions of oxidative stress *in vivo*, the oxidation pathways in the latter systems have not been unambiguously characterized and may involve multiple pathways depending on the experimental conditions (*16*). Therefore we have utilized for this study the thermal decomposition of an azo-initiator which yields well-defined species in predictable quantities and have described the oxidation products in order to elucidate the mechanism of Ca^{2+}-ATPase inactivation.

EXPERIMENTAL PROCEDURES

Materials. AAPH was obtained from Eastman Kodak Co. (Rochester, NY). HPLC grade solvents were purchased from Fisher Scientific Co. (Medford, MA). Other chemicals were of the highest commercial grade available. To remove traces of transition metals all buffers were treated with Chelex 100 chelating resin (Bio-Rad, Richmond, CA) as previously described (*17*).

Membrane Preparations. Native SR vesicles were prepared from rabbit skeletal white (fast twitch) muscle, essentially as described previously (*18*). Further purification by non-solubilizing concentrations of deoxycholate in the presence of high salt concentrations was performed by the method of Warren et al. (*19*). Protein concentration was determined according to Lowry et al. (*20*) or by the biuret method (*21*), using bovine serum albumin (BSA) as the standard.

Functional Assays. Oxidant-exposed membranes were diluted 80-fold into a medium containing 0.1 M KCl, 5 mM $MgCl_2$, 4 μM A23187, 25 mM MOPS (pH 7.0), 5 mM ATP, 1 mM EGTA, or 0.1 mM $CaCl_2$ for immediate assay of ATPase activity [measured at 25 °C by a calorimetric determination of inorganic phosphate released from vesicles (*22*)]. Determination of calcium-dependent ATPase activity required subtraction of activity assayed in the presence of EGTA (basal activity) from that assayed in the presence of $CaCl_2$ (total ATPase activity).

Polyacrylamide Gel Electrophoresis. Protein samples exposed to AAPH were diluted at least 10-fold into denaturing buffer immediately before application to sodium dodecyl sulfate polyacrylamide gel electrophoresis (SDS−PAGE) performed using 7.5% separating gels, according to the method of either Weber and Osborne (*23*) or Laemmli (*24*). To perform separation under reducing conditions, samples were dissolved in a Laemmli sample buffer in the presence of 2.5% β-mercaptoethanol and heated for 5 min at 40 °C before they were applied to the gel. Gels were stained for protein with Coomassie Blue R-250. The relative amount of monomeric and aggregated Ca^{2+}-ATPase was determined from densitometric measurements (FB 910 Densitometer, Fisher Scientific) of the protein bands.

Determination of Free Sulfhydryl Groups. The sulfhydryl concentration in SR vesicles was determined by measuring the increase in absorbance at 412 nm after reaction with 5,5′-dithiobis(2-nitrobenzoic acid) (DTNB), as described previously with modifications (*25,26*). SR protein (100 μg/mL) was suspended in 10 mM potassium phosphate (pH 7.3) containing 2.5% (w:w) SDS. Thereafter a final concentration of 200 μM DTNB was added into a total volume of 1 mL. The absorbance at 412 nm was measured after 30 min of incubation at 37 °C. A standard curve was established by addition of 10−100 μM glutathione (GSH, reduced form) to 200 μM DTNB in 10 mM potassium phosphate (pH 7.3) containing 2.5% SDS.

Oxidation Conditions. The incubation mixture contained 4 mg/mL of native or purified SR protein, 10 mM potassium phosphate (pH 7.3), 100 mM NaCl. The oxidative reactions were performed under air in glass test tubes immersed in a water bath maintained at 37 °C. The oxidation was initiated by the addition of different concentrations of AAPH [stock solution 0.5 M in 10 mM phosphate (pH 7.3) buffer] or 10 mM H_2O_2. After different times of incubation the reaction was stopped by separating protein from oxidant with a Sephadex G-50 column, eluting with 5% NaN_3 in water. Protein fractions were pooled and dried on a Centrivap (Labconco, Kansas City, MO) tabletop centrifuge and stored for further experiments. Specifically in the case of measurements of ATPase activity and SDS−PAGE, oxidation was curtailed by 10−80-fold dilution of protein into the appropriate (cold) media followed by immediate assay (see specific details in each section).

Fluorescence Measurements. All fluorescence measurements were done using a Perkin Elmer MPF-44B spectrofluorometer. The decrease in intrinsic fluorescence of SR membranes exposed to AAPH was measured between 375 and 500 nm with excitation at 275 nm (tyrosine and tryptophan) or 298 nm (tryptophan-specific). Bityrosine

formation was measured via excitation at 325 nm and emission at 375−500 nm (*27*).

Measurement of Lipid Peroxidation. Lipid peroxidation was assessed by quantitation of malondialdehyde, measured by HPLC separation of its corresponding 2,4-dinitrophenylhydrazone (DNPH) derivative (*28*). These measurements involved derivatization of 1 mg of oxidized SR protein with 3 μmol of DNPH (a total volume of 1 mL) followed by extraction with 1 mL of a hexane:methylene chloride (80:20, v/v). The extracts were evaporated and reconstituted with 0.1 mL of a hexane:acetonitrile mixture (60:40, v/v). An aliquot of 0.01 mL of this solution was injected into the ISCO 2350 HPLC apparatus equipped with a 5 μm C_{18} ISCO column (4.6 × 250 mm) and eluted isocratically with acetonitrile:water (60:40, v/v) at 1 mL/min. The malondialdehyde hydrazone was detected at 307 nm and eluted with a retention time of 4.6 min.

Susceptibility to Tryptic Hydrolysis. The susceptibility of oxidant-exposed membranes to tryptic digestion was assessed as described by Rupley (*29*) with the following modifications. 4 mg/mL of modified protein was incubated with 0.08 mg/mL of trypsin (1:50 trypsin:protein) at 30 °C in 50 mM ammonium carbonate (pH 8.5) buffer containing 100 μM $CaCl_2$ and 1 mM DTT. At different times, from 0 to 15 min, 0.5 mL aliquots were removed from the incubation mixture and trichloroacetic acid (TCA) was added to a final concentration of 5% (v/v). The residual protein was precipitated by centrifugation for 30 min, at 6000*g*. TCA-soluble peptides were measured using the Pierce BCA micro-protein assay (Rockford, IL).

Assessment of Protein Fragmentation. The fragmentation of SR proteins after incubation of SR vesicles with 75 mM AAPH at 37 °C for 2 h under standard oxidation conditions was assessed by measuring trichloroacetic acid soluble protein fragments. TCA was added to the oxidation reaction at a ratio of 1:1 (v/v) of 10% TCA:reaction mixture. After centrifugation for 30 min at 10000*g*, protein in the supernatant was measured using the Pierce BCA micro-protein assay (Rockford, IL). Parallel measurements were made in the absence of AAPH to control for any effects of incubation at 37 °C.

Tryptic Digestion. Digestion with trypsin for HPLC separation of peptide fragments was carried out essentially as previously described (*30*) in a mixture containing 4 mg of SR protein/mL, 0.08 mg of trypsin/mL (trypsin:SR protein ratio of 0.02), 50 mM NH_2HCO_3 (pH 8.5), 1 mM dithiothreitol, and 0.1 mM $CaCl_2$. After 2 h at 37 °C, 5 mM iodoacetic acid was added, and the incubation was prolonged for an additional hour. The reaction was finally quenched by a 5-fold dilution with cold water and centrifugation at 200000*g* for 90 min. The supernatant was collected and dried on a Centrivap tabletop centrifuge for purification by HPLC.

HPLC Separation of Tryptic Peptides. Separation of the soluble tryptic peptides from the supernatant was carried out on a Shimadzu HPLC system equipped with either a 4.6 × 250 mm Vydac C_4 or a SGE C_{18} reversed-phase column. First, dried peptides were redissolved in 10 mM ammonium acetate (pH 5.5) and injected onto the C_4 column, which had been equilibrated with 10 mM ammonium acetate (pH 5.5) (mobile phase A). After isocratic elution for 5 min with 95% mobile phase A, the peptides were eluted with a linear gradient of mobile phase B [10 mM ammonium acetate (pH 5.5), 10% water, 90% acetonitrile], from 5% to 60% within 60 min (flow rate 1 mL/min). The peptides were monitored by absorbance at 214 nm or by fluorescence intensity at 410 nm (excitation at 285 nm). 0.5 mL fractions of peaks I−V (see Figure 8) were collected for the second step of purification on a C_{18} column. After lyophilization, they were dissolved in mobile phase A′ (0.1% trifluoroacetic acid in water) and eluted with a linear gradient of 1%−95% mobile phase B′ within 98 min at 1 mL/min (B′: 0.1% trifluoroacetic acid in water, 90% acetonitrile). Peptide fractions were dried on a Centrivap tabletop centrifuge and subjected to sequencing and amino acid analysis (see below).

Mass Spectrometry. To obtain an independent evidence for bityrosine formation in the presence of AAPH, we used the tyrosine-containing peptide leucine enkephalin (Y-G-G-F-L). After oxidation of 10 mM peptide for 1 h (see oxidation conditions above) with 75 mM AAPH, peptide products were resolved on a C_4 reversed-phase HPLC, collected, and evaporated to dryness for MS analysis. Mass spectra were obtained on an AUTOSPEC-Q tandem hybrid mass spectrometer (VG Analytical Ltd, Manchester, U.K.) equipped with an OPUS data system and a continuous flow fast atom bombardment (cfFAB) probe. The sample was dissolved in MeOH/glycerol/water (75:5:20, v:v) and placed in the cfFAB probe reservoir for infusion into the mass spectrometer at ca. 5 μL/min with He pressure. The source temperature was 55 °C. Ionization was by a cesium ion beam from a gun operated at 20 keV energy and 2 μA emission. Spectra were acquired in continuum mode. The FAB and cfFAB analysis of peptides has been used to obtain sequence information; cfFAB conditions (*31*) have been optimized to obtain sequence indicative fragment ions using tens of picomoles of peptide.

Spectrophotometry of Bityrosine. To quantify bityrosine formation in the presence of AAPH, we used bityrosine standard spectra obtained in 5 mM sodium phosphate (pH 9.8) buffer containing 100 mM KCl (*32*). Spectra of the oxidation mixture consisting of 20 mM AAPH and 0.18 mg/mL of SR protein were digitally recorded at 10 min intervals with a Beckman DU-7500 spectrophotometer and subsequently subtracted from the background spectra of AAPH alone in the same buffer. The resulting difference spectra showed absorbance characteristic of standard bityrosine and were quantified using $\epsilon_{320} = 5500\ M^{-1}\ cm^{-1}$ (*32*).

Peptide Sequencing and Amino Acid Analysis. Peptide sequencing was provided by Commonwealth Biotechnologies, Inc. (Richmond, VA). The procedure utilized an automated phenyl isothiocyanate chemistry on a Hewlett Packard model G-1005A protein sequencing system and an Applied Biosystems model 470 gas phase sequencer with a dedicated model 120A PTH amino acid analyzer. The amino acid analysis was done by Commonwealth Biotechnologies Inc. (Richmond, VA) on a Hewlett Packard Amino Quant pre-column amino acid analysis system and a St. John's Associates post-column amino acid analyzer.

RESULTS

Effect of AAPH on Ca^{2+}-ATPase Activity. Incubation of native SR vesicles with increasing concentrations of AAPH at 37 °C results in increasing rates of Ca^{2+}-ATPase inactivation reaching a plateau at 75 mM (Figure 2, inset). The time course of inactivation at AAPH concentrations of 75 mM (shown in Figure 2) and lower is exponential. Incubation of SR vesicles at the same conditions but without AAPH

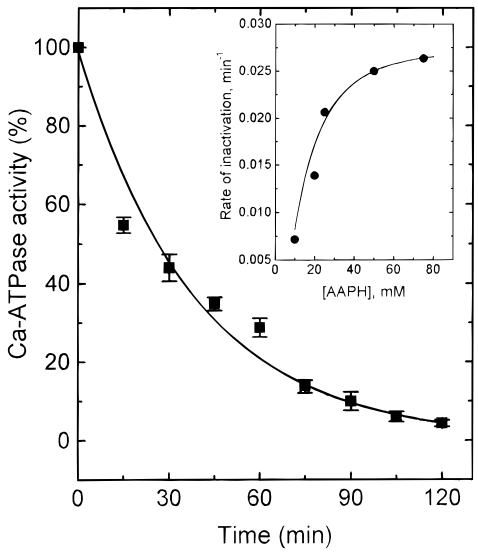

FIGURE 2: Ca^{2+}-ATPase inactivation by AAPH. SR vesicles (4 mg/mL) were incubated at 37 °C with 10 , 20, 25, 50, and 75 mM AAPH in 10 mM potassium phosphate (pH 7.3), 100 mM NaCl. At the indicated times, aliquots were withdrawn and assayed for ATPase activity. Calcium-dependent ATPase activity is plotted as a function of time for 75 mM AAPH; the solid line is the result of the fit to a single exponent. For inactivation at other AAPH concentrations, linear regression fits to the data from plots of ln of activity as a function of time were used to determine inactivation rates; these are plotted in the inset. Ca^{2+}-ATPase activities of 100% correspond to values of 2.96 ± 0.07 μmol of P_i min^{-1} (mg of protein)$^{-1}$ (mean ± SD, $n = 7$) for native SR vesicles.

does not result in inactivation of Ca^{2+}-ATPase activity. Complete inactivation is observed only after 2 h of incubation at the highest concentration of AAPH employed (75 mM), which corresponds to a maximal free radical concentration of 702 μM as calculated from eq 4.

AAPH-Induced Protein Aggregation. We examined the possibility of radical-induced cross-linking or fragmentation of the Ca-ATPase using SDS−PAGE under reducing conditions (Figure 3). Incubation of SR vesicles with AAPH results in a time-dependent loss of monomeric (100 kDa) Ca^{2+}-ATPase which fits well to a single exponent. Concomitantly we observe a progressive accumulation of higher molecular weight species that do not enter the gel, suggesting the presence of either covalently cross-linked or tightly but non-covalently associated protein. The small amount of 200 kDa protein, corresponding to incompletely solubilized Ca^{2+}-ATPase dimers in the native preparation (Figure 3A, lane 1), increases at early time points of oxidation and subsequently disappears, suggesting an oxidant-induced transient intermediate in larger aggregate formation. The relative abundance of higher molecular weight aggregates increases approximately 5-fold after 2 h of incubation with AAPH, accumulating with a time course that correlates well with Ca^{2+}-ATPase inactivation. The persistence of aggregates on SDS−PAGE under reducing conditions indicates that these higher molecular weight aggregates do not result from the formation of intermolecular disulfide cross-links. Moreover, on non-reducing SDS−PAGE no additional high molecular weight aggregates are observed, ruling out any significant formation of intermolecular disulfides (data not shown). Determination of trichloroacetic acid-soluble peptides after oxidation also rules out any radical-induced fragmentation of the Ca-ATPase polypeptide chain corresponding to more than 2% of total protein, nor do low molecular weight peptides appear on SDS−PAGE after oxidation (Figure 3A).

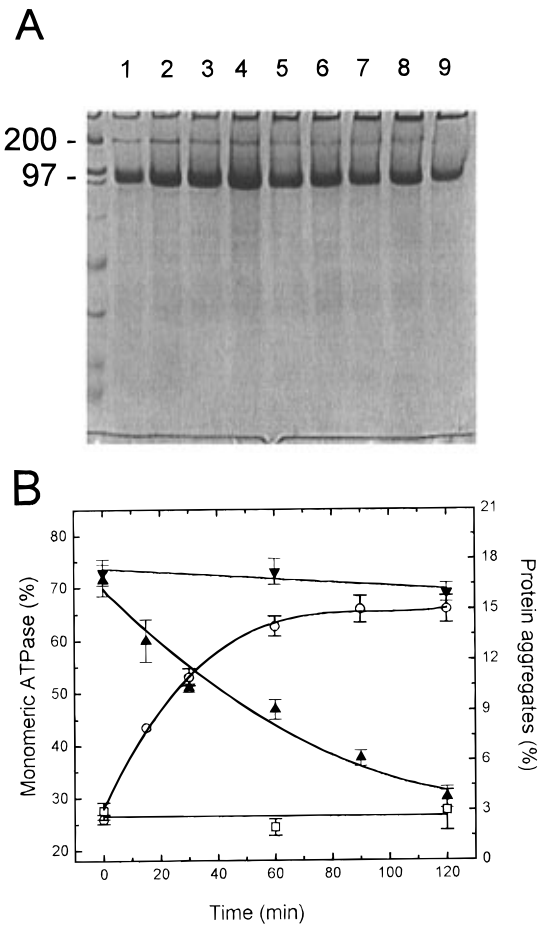

FIGURE 3: AAPH-induced changes in Ca^{2+}-ATPase association in SR vesicles. (A) SDS−PAGE (with 2.5% β-mercaptoethanol) of SR vesicles after exposure for various times to 75 mM AAPH at 37 °C. Lanes 1−9 contain samples exposed for different times to AAPH, i.e., 0, 15, 30, 45, 60, 75, 90, 105, and 120 min, respectively. (B) Results of densitometer scans after various times of exposure to AAPH shown. The abundance of the 100 kDa monomeric Ca-ATPase relative to the total SR proteins is shown in the presence (▲) or absence (▼) of AAPH in the incubation medium. The relative abundance of higher molecular weight proteins that do not enter the gel are shown as a result of the presence (○) or absence (□) of AAPH in the medium. Data represent the mean ± SD of five independent determinations.

Formation of Bityrosine. The AAPH-induced formation of a fluorescent species with an emission maximum at 420 nm, characteristic of the emission of bityrosine, has been observed both from the SR Ca-ATPase and tyrosine alone after exposure to AAPH (Figure 4A) (*27*). Unoxidized SR does not emit in this region (390−500 nm) when excited at 325 nm, demonstrating that the measured fluorescence does not originate from intrinsic fluorescent groups, e.g., tryptophans or tyrosines. The time course of the formation of this fluorescent species (Figure 4B) closely parallels the formation of large aggregates (Figure 3), suggesting that aggregate formation results from bityrosine cross-links.

In order to confirm that the fluorescence signal observed after exposure of SR to AAPH was derived from bityrosine, independent evidence was obtained that tyrosine-containing peptides are capable of forming fluorescent bityrosine cross-links in the presence of AAPH. Further chemical evidence by HPLC for the formation of bityrosine from the Ca^{2+}-ATPase is presented below. Leucine enkephalin (Y-G-G-F-L) was chosen as a model because of its modest mass (555.27 amu), excellent FAB sensitivity, and known MS fragmentation behavior (*33*). We performed AAPH-induced

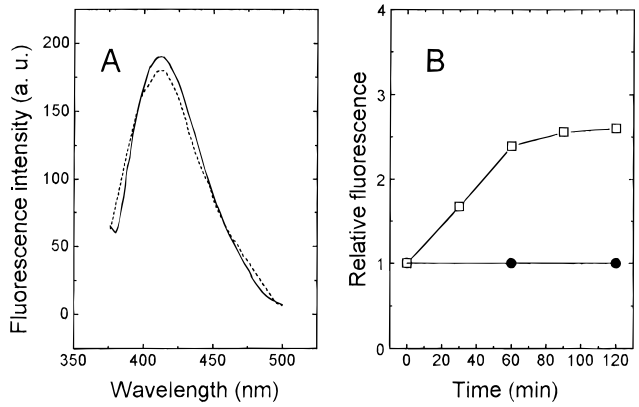

FIGURE 4: AAPH-induced appearance of bityrosine fluorescence in purified SR vesicles. (A) Emission spectra (λ_{ex} = 325 nm) after exposure of 0.5 mM tyrosine to 75 mM AAPH for 120 min (solid line) or SR membranes incubated at 37 °C for 120 min in the presence of 75 mM AAPH (enlarged × 3, dashed line). (B) Time course of bityrosine formation during incubation of purified SR vesicles with 75 mM AAPH, as described in Experimental Procedures: SR vesicles with (□) or without (●) AAPH. Bityrosine formation was monitored by emission at 420 nm (λ_{ex} = 325 nm). Fluorescence values are plotted relative to the values at 0 min exposure to AAPH and represent the means of three independent determinations for which standard errors were less than 5%.

oxidation of leucine enkephalin, subsequently resolving two peptide peaks on C_4 reversed-phase HPLC: the first peak had a retention time of 19 min, identical to that of unreacted leucine enkephalin, and the second peak had a retention time of 23.5 min and a fluorescence spectrum characteristic of bityrosine. The cfFAB analysis of the latter peak exhibited the spectrum shown with an abundant ion observed at *m/z* 1109.4 (Figure 5A). The predicted protonated (MH^+) mass of a peptide formed from the bityrosine coupling of YGGFL is 1109.5 amu [2 × 555.27 (YGGFL) − 2 × 1.008 (H) + 1.008 (H^+)] (*34*). The cfFAB spectrum of the fluorescent HPLC peak contains numerous nonmatrix ions above *m/z* 650. If the A, B, (C+2H) and X, (Y+2H), Z type fragment ions (see *35* for nomenclature) are calculated for the sequence depicted in Figure 5B, the MS data clearly substantiate coupling of the peptide through tyrosine. A complete (*C*+2H) series is evident, and some A ions are observed. A possible coupling of peptide through phenylalanine is precluded by noting a significant *m/z* 120 ion in the low-mass region (not shown) characteristic of unmodified Phe. Further, there is no *m/z* 136, which would correspond to the A1 or Tyr immonium in the spectrum of unmodified Tyr in YGGFL (*33*).

From UV/vis spectra (*32*) we estimate the maximum amount of bityrosine formed in SR after 2 h of exposure to AAPH as 8.44 nmol/mg of SR protein, corresponding to a molar ratio of bityrosine:Ca-ATPase of 1.3 based on the relative abundance of the Ca^{2+}-ATPase on SDS−PAGE (i.e., 72% ± 4%) and assuming that other SR proteins do not form bityrosine. This level of bityrosine is consistent with (i) the intermolecular formation of bityrosine between 50% of the total Ca^{2+}-ATPase polypeptide chains (i.e., 0.25 bityrosine per Ca^{2+}-ATPase) and (ii) the additional formation of approximately one bityrosine per Ca^{2+}-ATPase polypeptide

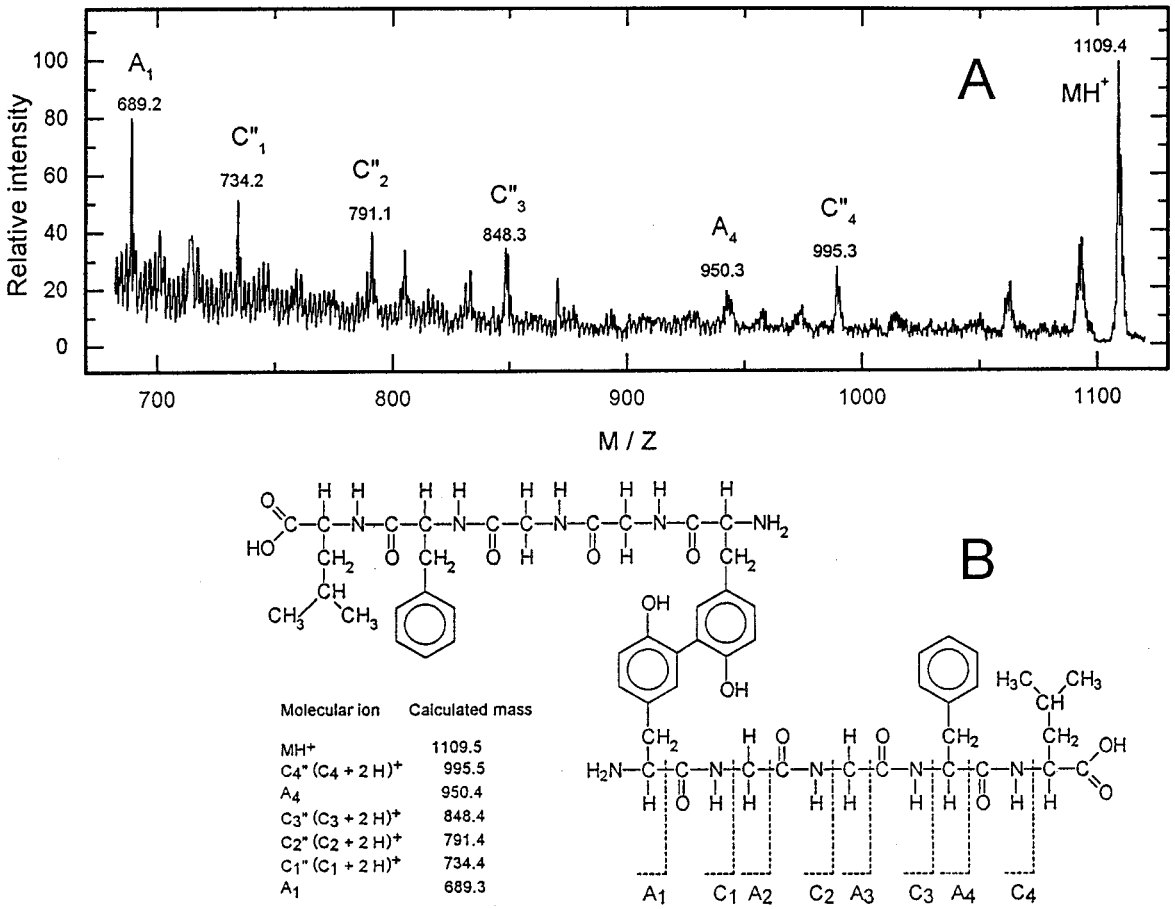

FIGURE 5: Mass spectrometric evidence for bityrosine formation in AAPH-treated leucine enkephalin (Y-G-G-F-L) peptide. (A) cfFAB spectrum in the 680−1120 *m/z* range. Sequence ions are indicated with respect to the structure depicted in B. (B) Predicted structure of tyrosine-coupled Y-G-G-F-L dimer shown with the fragmentation pattern, characteristic for A and C type ions (*35*). Calculated masses for A and C+2H^+ ions are shown in the adjoining table.

Table 1: Changes in Amino Acid Composition of Skeletal Muscle SR Protein after Oxidation By AAPH[a]

amino acid	change after reaction	amino acid	change after reaction
Arg	−9.3 ± 1.2	Ile	+4.4 ± 0.2
As(x)[b]	+8.0 ± 0.45	Lys	−14.2 ± 0.8
His	−2.8 ± 0.2	Met	−15.6 ± 1.3
Gl(x)[b]	+29.0 ± 0.8	Trp	−4.5 ± 0.2
Thr	−14.8 ± 1.3	Tyr	−1.8 ± 0.2

[a] Purified SR membranes were exposed to 75 mM AAPH for 120 min at 37 °C, and analysis was performed as described in Experimental Procedures. All values are in nmol per mg of SR protein (the Ca^{2+}-ATPase content is 72% ± 4% of total SR protein, based on SDS−PAGE densitometry). Data represent the mean (±SD) of four independent determinations. [b] As(x) refers to Asp and Asn; Gl(x) refers to Glu and Gln.

chain, as described below.

Oxidative Modification of the SR Protein. In order to detect other oxidative modifications of the protein, changes in compositions of the native and modified SR proteins were assessed by amino acid analysis, as shown in Table 1. The exposure of SR to AAPH leads primarily to the loss of significant amounts of Arg, His, Lys, Met, Thr, and Tyr residues. Accompanying the loss of some amino acid residues is an increase in the abundance of As(x), Gl(x), and Ile. The oxidative modification of cysteines was determined by titration with DTNB (see below). The modification of Trp, assayed by amino acid analysis following alkaline hydrolysis (Table 1), revealed a substantial loss of tryptophans.

Inactivation of Ca^{2+}-ATPase and Cysteine Modification. In order to explore the possible involvement of cysteine modification in Ca^{2+}-ATPase inactivation, the effect of AAPH on the number of accessible free sulfhydryl groups was determined by reaction of DTNB with purified SR vesicles (Figure 6). The number of DTNB-reactive SH groups after solubilization in SDS (20-21) is in good agreement with previous measurements (*10*, *26*) and indicates that under these assay conditions a substantial fraction of the total 24 sulfhydryls of the Ca^{2+}-ATPase are accessible to DTNB (*36*). While no significant changes are observed in the absolute number of free sulfhydryl groups due to incubation of SR vesicles at 37 °C, exposure of SR to AAPH at 37 °C for up to 2 h results in a 50% decrease in the number (10) of free sulfhydryl groups, suggesting their oxidative modification. However, only a fraction of the modified cysteine residues is involved in Ca^{2+}-ATPase inactivation as indicated by experiments utilizing mild oxidizing conditions, i.e., 15 min of exposure to 20 mM AAPH, in which a loss of 5.2 sulfhydryl groups results in no significant loss in enzyme activity (data not shown). This result is in agreement with the earlier observation that the oxidation of up to six sulfhydryl groups has little influence on the activity of Ca^{2+}-ATPase (*37*).

Protection of SR Ca^{2+}-ATPase Oxidation by Exogenous Amino Acids. In light of these multiple oxidative modifications of the Ca^{2+}-ATPase we examined the ability of several oxidation susceptible amino acids to protect the Ca^{2+}-ATPase from inactivation (Figure 7A). We find that the addition of 0.5 mM histidine, lysine, cysteine, methionine, or tryptophan to the incubation mixture has no effect on the rate or the extent of Ca^{2+}-ATPase inactivation by AAPH. Only the presence of 0.5 mM tyrosine completely prevents Ca^{2+}-ATPase inactivation up to 90 min exposure to AAPH,

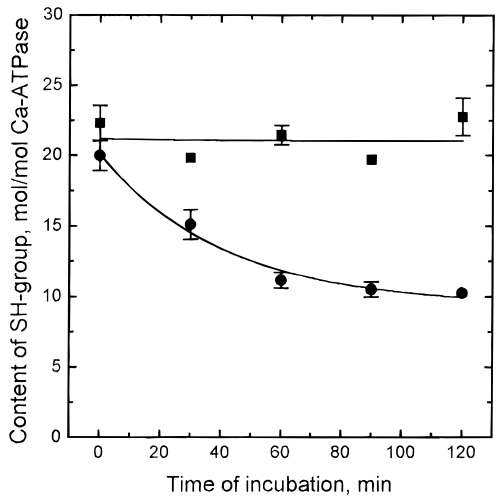

FIGURE 6: Changes in the amount of DTNB-accessible sulfhydryl groups in purified SR membranes after incubation with AAPH. Sulfhydryl groups (SH groups/mol of Ca^{2+}-ATPase) were determined after incubation of purified SR membranes at 37 °C in the absence (■) and in the presence (●) of 75 mM AAPH. SR (100 μg/mL) was incubated in 10 mM potassium phosphate (pH 7.3), 2.5% SDS, for titration of sulfhydryl groups with DTNB as described in Experimental Procedures. Data represent the mean (±SD) of five independent experiments. Determination of the number of free sulfhydryls/mol Ca^{2+}-ATPase was based on the assumptions that (i) each mg of purified SR contains 72% ± 4% Ca^{2+}-ATPase, based on the densitometry of SDS−PAGE, and that (ii) 95% of all sulfhydryls in SR proteins reside on the Ca^{2+}-ATPase (*55*).

suggesting the effectiveness of tyrosine as a radical scavenger and that oxidation of one or more tyrosine residues may be a primary event responsible for the loss of Ca^{2+}-ATPase activity. At the same time 0.5 mM tyrosine substantially, but not completely, reduced the associated cross-linking (Figure 7B).

On the other hand, complete protection of Ca^{2+}-ATPase activity by tyrosine results in no significant alteration in the content of malondialdehyde, a commonly assayed marker of lipid peroxidation (Figure 7C). Malondialdehyde was observed to accumulate linearly (up to 4 mol % of SR lipid concentration) during 2 h of incubation at 37 °C in the presence of 75 mM AAPH with rates of 60.7 ± 7.5 and 52.0 ± 4.1 pmol min^{-1} (mg of SR protein)$^{-1}$ in the absence and presence of 0.5 mM tyrosine, respectively. Thus the small amount of AAPH-induced lipid peroxidation is not mechanistically related to inactivation of the Ca^{2+}-ATPase.

HPLC Separation of Tryptic Peptides. In order to identify oxidatively modified sites within the Ca^{2+}-ATPase sequence, tryptic digests were separated by HPLC for identification by N-terminal sequencing and amino acid analysis. Figures 8A−C show the tryptic peptide maps obtained by reversed-phase HPLC on a Vydac C_4 column. Although substantially fewer than the 93 peaks predicted from the abundance of proteolytic sites in the amino acid sequence of the Ca^{2+}-ATPase (*36*) are produced, these conditions nevertheless provide a convenient and reproducible peptide map for initial isolation of modified peptides. Oxidation by AAPH results in substantial changes in the relative abundance of five peptide-containing peaks (see Figures 8 and 9). Fractions from each peak from the C_4 column were collected for further purification on a C_{18} column. As an example, Figure 8D shows that peak IV collected from the C_4 column contained 25% of another peptide, which is successfully resolved by subsequent chromatography on a C_{18} column. The purified

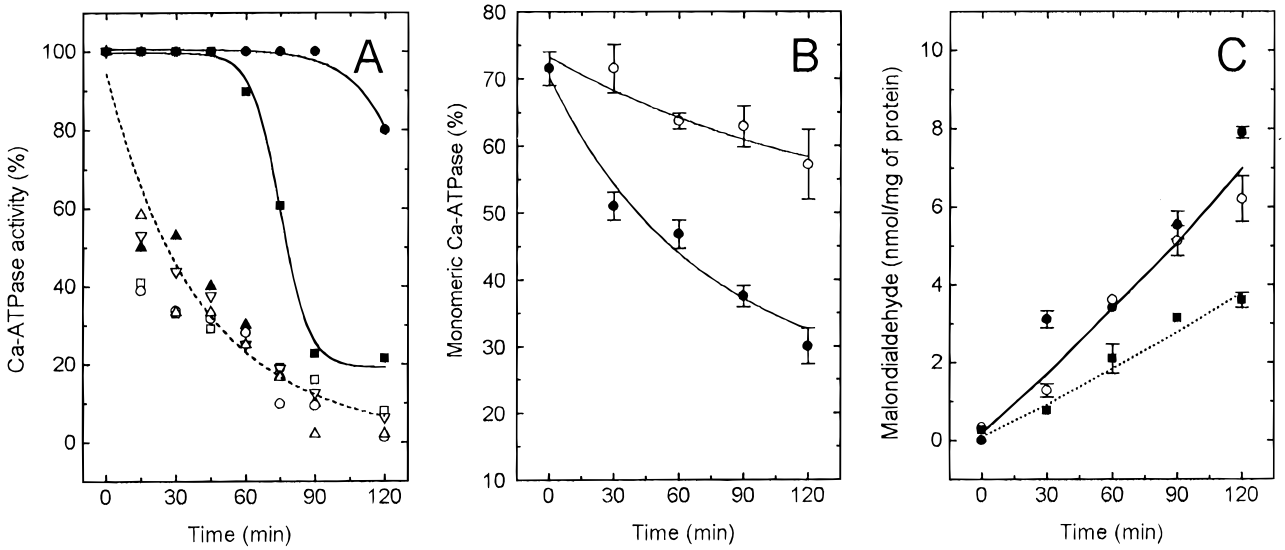

FIGURE 7: AAPH-stimulated oxidation in SR membranes: protection by various amino acids. (A) The influence of 0.1 mM (■) tyrosine or 0.5 mM tyrosine (●), tryptophan (▲), histidine (▽), cysteine (□), methionine (○), or no added amino acid (△) on Ca^{2+}-ATPase activity in SR vesicles exposed to 75 mM AAPH for times up to 120 min at 37 °C as described in Experimental Procedures. Ca^{2+}-ATPase activity values of 100% correspond to values of 2.96 ± 0.07 μmol of P_i min^{-1} (mg of protein)$^{-1}$. Values are means of three independent determinations for which standard errors were less than 5%. (B) Content of monomeric Ca^{2+}-ATPase protein determined from densitometry of purified SR protein separated on SDS−PAGE after oxidation by AAPH (75 mM) in the presence (○) and absence (●) of 0.5 mM tyrosine. Data represents the means (±SD) of three independent determinations. (C) Content of malondialdehyde in native SR vesicles (■) and in purified SR vesicles [in the presence (○) and absence (●) of 0.5 mM tyrosine] after various times of exposure to 75 mM AAPH. Data represent the means (±SD) of three determinations.

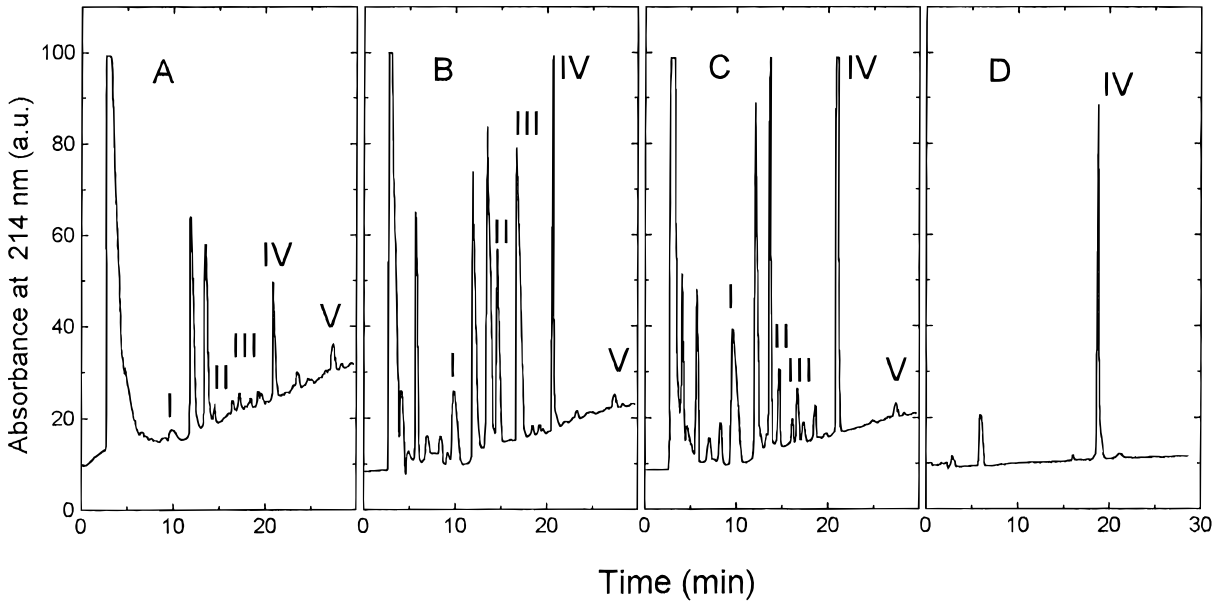

FIGURE 8: Separation of tryptic SR vesicles peptides by reversed-phase HPLC on C_4 (panels A−C) and C_{18} (panel D) columns. Soluble tryptic peptides derived from 1 mg of purified SR vesicles in were dissolved in 100 μL of 10 mM ammonium acetate (pH 5.5), injected onto a Vydac C_4 column (4.6 × 250 mm), and eluted as decribed in Experimental Procedures. Peptides were detected by UV at 214 nm; peak V is enlarged four times to clarify presentation. (A) Native Ca^{2+}-ATPase. (B) 60 min incubation with 10 mM H_2O_2. (C) 60 min incubation with 75 mM AAPH. Fractions I (t_R = 10.07 min), II (t_R = 15.5 min), III (t_R = 17.2 min), IV (t_R = 21.2 min), and V (t_R = 26.0 min) were collected (0.5 mL) and retained for further purification. (D) Fraction IV from the chromatogram shown in panel C was rechromatographed on an SGE C_{18} column (4.6 × 250 mm) as decribed in Experimental Procedures.

fractions from the C_{18} column were identified by N-terminal sequencing and amino acid analysis (see below).

Oxidative Damage Induced by Hydrogen Peroxide. For comparison, we also examined the HPLC profile of tryptic peptides resulting from exposure of SR to H_2O_2, another reactive oxygen species of similar reaction mechanism as that of AAPH-derived organic peroxides (*38*). Table 2 summarizes the effects of H_2O_2 on Ca^{2+}-ATPase activity and Ca^{2+}-ATPase monomer content, showing that similar to AAPH-induced oxidation, loss of monomeric species correlates with protein inactivation. Oxidation by H_2O_2 also results in significant increases in the relative abundance of five proteolytic peptides having the same retention times as those whose abundance is altered by AAPH (Figure 8B). Peaks designated I, IV, and V exhibit nearly identical time courses of appearance and disappearance, while those of peaks II and III differ depending on the particular oxidant (Figure 9). Although we have not identified the precise modifications of each peptide peak induced by H_2O_2, these patterns emphasize the different kinetics of oxidation by H_2O_2 or AAPH of the same oxidatively-sensitive regions of the Ca^{2+}-ATPase.

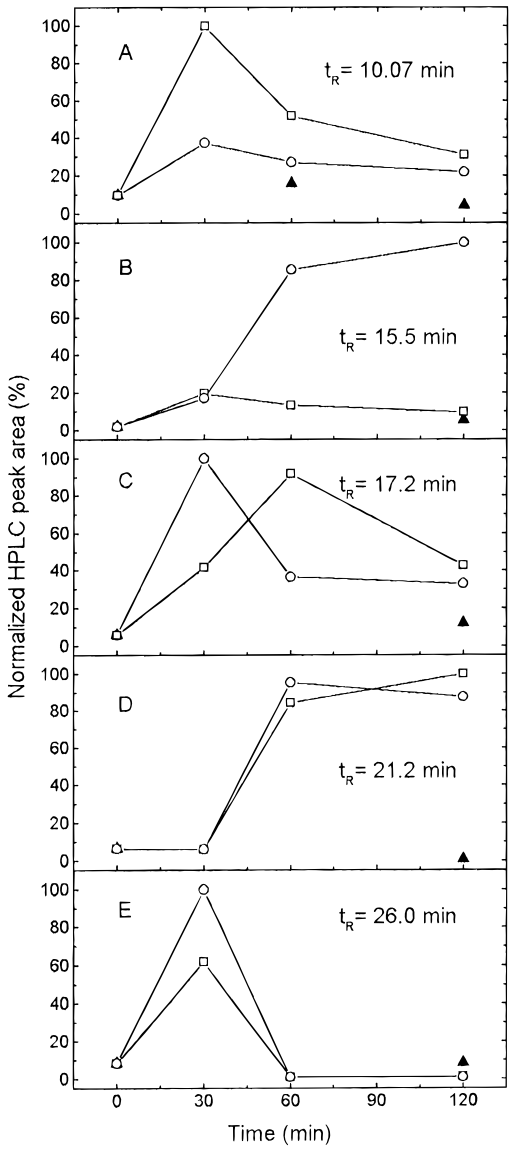

FIGURE 9: Changes in the content of tryptic peptides of SR vesicles as a result of oxidation by 75 mM AAPH (□), 10 mM H_2O_2 (○), or control [no oxidant added (▲)] at various times of incubation up to 2 h. Tryptic peptides are identified in Figure 8 and denoted by retention times (t_R) on C_4 reversed-phase HPLC. HPLC peak areas were normalized on the largest area of the selected H_2O_2- or AAPH-oxidized peak. Each data point represents an average of five determinations.

Table 2: Effect of 10 mM H_2O_2 on Ca^{2+}-ATPase Activity and Amount of Monomeric Band of Ca^{2+}-ATPase

time of incubation	Ca^{2+}-ATPase activity[a] (μmol P_i/min/mg of protein)	content of monomeric band[b] (%)
0 min	2.96 ± 0.07	68.1
30 min	2.54 ± 0.05	62.2
60 min	2.50 ± 0.06	64.1
90 min	2.01 ± 0.05	63.2
120 min	2.11 ± 0.05	54.7

[a] Data represent the mean (±SD) of three determinations. [b] Based on densitometry of SDS−PAGE. Data are the mean of two different analyses from a representative experiment.

Sequencing and Identification of Purified Peptides. The sequencing of purified proteolytic peptides obtained from chromatographic fractions (peaks I−V, Figure 8C) allows their assignment to the primary sequence of the Ca^{2+}-ATPase (*36*; Figure 10) and gives further evidence for the formation of bityrosine. Rechromatography of peak I on a C_{18} column resolves three separate peaks. N-terminal sequencing identifies the first peak (t_R = 8.9 min, representing 56% of the total peptide eluted) as G_{432}-V-Y-E-K_{436}. A minor component (t_R = 13.1 min; 14% of the total protein) corresponds to that of the tryptic peptide E_{121}-Y-E-P-E-M-G-K_{128}. Both peptides exhibit intact amino acid sequences, unmodified by oxidation, but a third peak (t_R = 10.7 min, 30% of the total protein) also apparently contains tyrosine within its sequence, as shown by its bityrosine fluorescence. However, this peptide cannot be unambigously identified by sequencing as it does not yield a homogeneous sequence, suggesting a possible site of cross-linking between heterogeneous regions of the Ca^{2+}-ATPase.

N-terminal sequencing identifies the first six amino acids of the peptide purified from peak II as H_{190}-T-E-P-V-P. On the basis of the total amino acid analysis of this peak, this peptide extends through Lys_{218}. Amino acid analysis of peak II's peptide shows that after 2 h of oxidation two of the peptide's three Lys residues are lost, presumably due to their chemical modification. The modified lysines correspond to Lys_{203} and Lys_{204} based on the observation that the third and terminal lysine (Lys_{218}) represent an intact tryptic cleavage site. At the same time, the peptide's single arginine (Arg_{198}), the very sensitive (T_2) tryptic site of Ca^{2+}-ATPase, remains intact, suggesting a substantial decrease in its accessibility to trypsin. Additionally, the Gl(x) content increased from two to five residues.

Further purification of peak III yields two peaks: a major fraction (t_R = 27.3 min) and a minor fraction (t_R = 20.5 min). The major component is identified as a peptide starting with Glu_{551}, from an N-terminal sequence of E-W-G-T-G-R, and, on the basis of amino acid analysis, extending through Arg_{604}. The minor component is similarly identified as Glu_{551} through Lys_{572}, probably a further hydrolysis product of the major fragment. Amino acid analysis of peak III shows the loss of Met (two), Thr (three), Lys (one), Arg (two), and Trp (one) residues, with increases in Gly (five) and Gl(x) (seven). We note the presence of a single tyrosine residue (Tyr_{587}) in the native form of this sequence, suggesting that bityrosine cross-links may originate from this domain. In fact, fluorescence characteristic of bityrosine is observed in fragment III and confirmed by its acid hydrolyzate which exhibits a fluorescence peak having the same retention time during reversed-phase HPLC (Figure 11) as that of the bityrosine fluorescence peak derived from the acid hydrolyzate of AAPH-oxidized leucine enkephalin. In both cases these fluorescence peaks are the smallest fragments of peptide III and leucine enkephalin cross-links, are resistant to further acid hydrolysis, and thus represent a covalently linked Tyr dimer. The N-terminal sequencing (first six amino acids) of peak III gives a single sequence, suggesting that bityrosine is part of a symmetric cross-link of two Tyr_{587} on neighboring Ca^{2+}-ATPase polypeptide chains.

The single peptide purified from peak IV (Figure 8D) is identified from an N-terminal sequence of N-A-I-V-R-S as starting with Asn_{330} and, on the basis of amino acid analysis, extending through Lys_{352} (Figure 10). This peptide is part of a sequence (Lys_{328} to Thr_{357}) that is highly conserved among cation ATPases (*39*) and connects the enzyme's phosphorylation site (Asp_{351}) with one of the calcium transport sites (Glu_{309}). The single peptide from peak V is identified from an N-terminal sequence of E-F-D-D-L-P, and amino acid analysis, as a sequence starting with Glu_{657} and extending through Arg_{671} (Figure 10). Both peptides con-

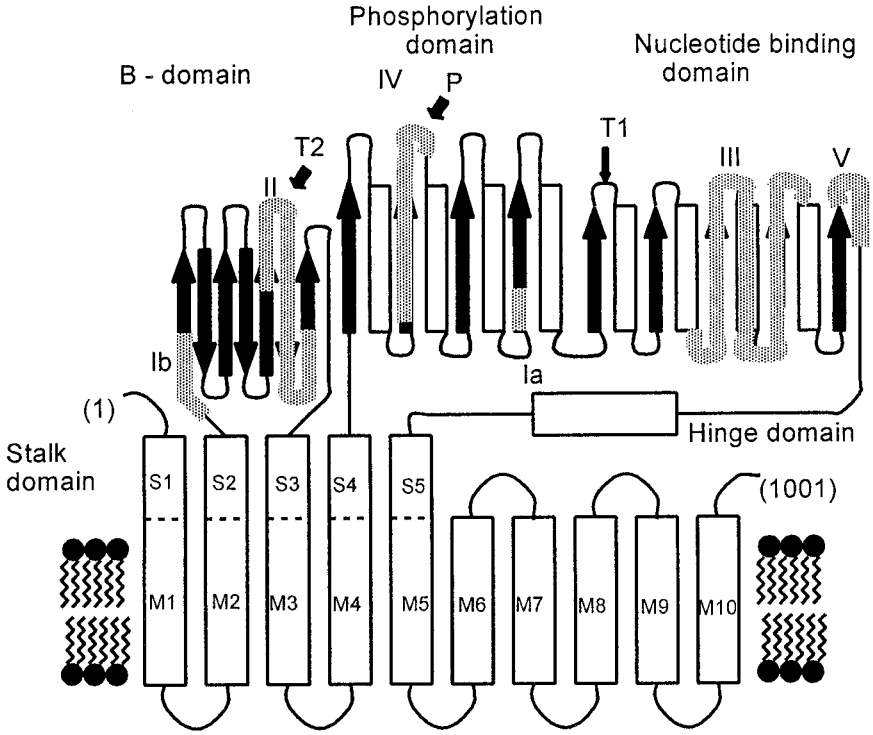

FIGURE 10: Structural diagram of the Ca^{2+}-ATPase molecule depicting peptides that are sensitive to AAPH oxidation. This diagram is based on the predicted tertiary structure of Ca^{2+}-ATPase (*52*, *56*) that includes β-structures (solid arrows) and α-helices (open rectangles) in cytosolic B-, phosphorylation, nucleotide binding, and hinge domains, five (S1−S5) stalk domain α-helices, and ten (M1−M10) transmembrane α-helices. Protein segments that protrude on the cytosolic side of the membrane contain six oxidatively sensitive peptides (shown as shaded areas) that were initially resolved from C_4 HPLC peaks I−V (Figure 8); their respective sequences are (Ia) G_{432} -V-Y-E-K_{436}, (Ib) E_{121}-Y-E-P-E-M-G-K_{128}, (II) H_{190}-T-E-P-V-P-D-P-R-A-V-N-Q-D-K-K-N-M-L-F-S-G-T-N-I-A-A-G-K_{218}, (III) E_{551}-W-G-T-G-R-D-T-L-R-C-L-A-L-A-T-R-D-T-P-P-K-R-E-E-M-V-L-D-D-S-S-R-F-M-E-Y-E-T-D-L-T-F-V-G-V-V-G-M-L-D-P-P-R_{604}, (IV) N_{330}-A-I-V-R-S-L-P-S-V-E-T-L-G-C-T-S-V-I-C-S-D-K_{352}, and (V) E_{657}-F-D-D-L-P-L-A-E-Q-R-E-A-C-R_{671}. Initial tryptic cleavage sites T_1 (Arg_{198}) and T_2 (Arg_{505}) as well as the enzyme's phosphorylation site P (Asp_{351}) are indicated by small arrows.

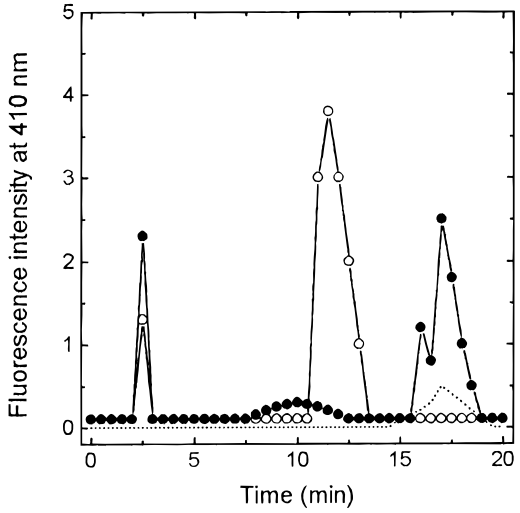

FIGURE 11: HPLC analysis of bityrosine in acid hydrolyzate of peptides: leucine enkephalin (Y-G-G-F-L) exposed to 75 mM AAPH at 37 °C for 2 h (●), tryptic peptide III, purified as described in Figure 8D (···), and intact leucine enkephalin (○). Acid hydrolyzates (6 N HCl, 6% thioglycolic acid, 24 h, 110 °C) of peptides were subjected to HPLC using an SGE C_{18} column (4.6 × 250 mm) and isocratic elution with 0.5% acetic acid−methanol (29:1, v/v) at a flow rate of 0.8 mL/min (*57*). Fluorescence detection at 410 nm (excitation at 285 nm) was used.

tained one potential cleavage site, i.e., Arg_{334} and Arg_{667}, respectively, which were intact in the oxidized enzyme. For both peptides (peaks IV and V) amino acid analysis accounts for all residues except cysteines, indicating that resolution of these peptides results from their altered proteolytic susceptibility rather than oxidative modification of some residues. It should be noted, however, that amino acid sequences of peaks III, IV, and V contain total four potentially oxidizable cysteine residues and, if converted by oxidation into polar sulfonic (sulfenic) acid residues, may facilitate proteolytic cleavage.

DISCUSSION

The current study was designed to examine the oxidative sensitivity of the SR Ca^{2+}-ATPase with the view that knowledge of its sensitivity to and its mechanism of oxidative inactivation may provide a rationale for understanding the loss of calcium homeostasis observed under conditions of oxidative stress. Our focus on the SR Ca^{2+}-ATPase stems from its primary role as the rate-limiting enzyme in the regulation of normal intracellular calcium transients responsible for excitation−contraction coupling in muscle. The sensitivity of this protein to oxidation is demonstrated by its appreciable loss of enzymatic activity as a result of exposure to even a few micromolar generated radicals (Figure 2). Although AAPH and its thermolytic products are not physiological molecules, their chemical reactivity with SR membrane components can be taken as representative of the wide variety of peroxyl and alkoxyl radicals derived from cellular biomolecules.

Formation of Bityrosine Cross-Links. The loss of Ca^{2+}-ATPase activity correlates with the cross-linking of polypeptide chains and the appearance of a fluorescence signal characteristic of bityrosine (Figures 2−4). That this fluorescence signal indeed originates from bityrosine was demonstrated by the following criteria: (i) Using mass spectrometry to identify the fluorescent product, we have

shown that tyrosine side chains in leucine enkephalin are capable of forming bityrosine in the presence of AAPH-derived radical species (Figure 5). (ii) Bityrosine derived from acid hydrolysis of oxidized leucine enkephalin co-elutes during reversed-phase HPLC with a product from Ca^{2+}-ATPase oxidation, which, on the basis of fluorescence measurements, was also identified as bityrosine (Figure 11). Bityrosines formed from tyrosines on neighboring Ca^{2+}-ATPase polypeptide chains would appear to explain the aggregate accumulation resulting from exposure to AAPH; the level of bityrosine is significant (1.3 mol/mol of Ca^{2+}-ATPase) and is sufficient to account for the observed (50%) loss of Ca^{2+}-ATPase monomer. Moreover, the time courses for aggregation and bityrosine formation are identical (Figures 3 and 4), and the presence of exogenous tyrosine during exposure to AAPH prevents most of the accumulation of protein aggregates while maintaining enzyme activity (Figure 7). The formation of intermolecular disulfide cross-links can be ruled out from both reducing and non-reducing SDS−PAGE (Figure 3).

The SR Ca^{2+}-ATPase has been previously shown to be particularly sensitive to cross-linking and the concomitant decrease in protein rotational mobility (*40*−*43*). Thus, the loss of Ca^{2+}-ATPase activity observed in this study (Figure 2) is, at least in part, accounted for by the loss of rotational mobility due to protein aggregation. However, complete enzyme inactivation coincides with retention of a substantial fraction of species that migrate as a monomer on SDS−PAGE indicating that inactivation involves additional mechanisms not involving irreversible protein cross-linking. One possibility is inactivation by an additional component of aggregation that is non-covalent and induced by bityrosine formation. Another possibility includes inactivation by one or more of the oxidative modifications of Lys, Arg, His, Met, Thr, Cys, and Trp residues (Table 1). In contrast to inactivation, covalent cross-linking is essentially complete within 60 min (Figure 3), suggesting that any additional inactivation processes occur with slower rates than that of bityrosine formation. Oxidative modifications involved in the appearance of peptides III and IV (Figure 9) require more than 60 min of exposure to AAPH and are, therefore, likely candidates, especially peptide III which exhibits numerous oxidative modifications in addition to bityrosine formation.

Possible Chemical Mechanisms of Oxidative Modifications. Consistent with general mechanisms reported for protein oxidation, we find that Lys, Arg, His, Met, and Trp residues of Ca^{2+}-ATPase are particularly sensitive to AAPH-induced oxidation (*13*, *16*, *44*). In addition, we demonstrated for the first time that AAPH-derived oxy radicals also cause both chemical modification of Thr residues and formation of bityrosine cross-links. Oxidative modifications that are functionally relevant are likely derived from the initial attack of the AAPH-derived peroxyl radical on a tyrosine residue of the Ca^{2+}-ATPase, since exogenous tyrosine is unique in its ability to prevent inhibition of activity (Figure 7). Previous work has provided evidence for chain reactions in the protein interior during oxidation; for example, it has been found that for oxidized BSA each initial radical of the protein in the presence of oxygen may be responsible for the chemical modification of approximately 15 additional amino acids (*45*). In the case of AAPH-induced oxidation of the Ca^{2+}-ATPase, we can conclude the presence of a small chain reaction based on the ratio of the concentration of initial radicals generated to the final concentration of oxidized amino acids. For example, taking the loss of each amino acid as determined by amino acid analysis after either acid or alkaline hydrolysis, we obtain a combined loss of approximately 64 amino acids for each Ca^{2+}-ATPase polypeptide chain. The 4 mg/mL of SR protein used in the oxidation reaction corresponds to 2.7×10^{-5} M Ca^{2+}-ATPase; thus the oxidation by AAPH of 64 (out of a total of 1001) amino acids produces 1.7×10^{-3} M oxidized amino acids. On the other hand, using $R_i = 1.36 \times 10^{-6}$ s^{-1} at 37 °C (*12*) the maximum possible concentration of initiating peroxyl radicals can be calculated to be 7.02×10^{-4} M for 2 h of exposure to 75 mM AAPH. Thus the ratio of oxidation products to initial radical amounts to 2.4, or greater, which is in agreement with a small chain reaction occurring within the protein. Such a chain reaction may be initiated by a tyrosyl peroxyl radical; the formation of the latter has been suggested for various proteins, e.g., in prostaglandin endoperoxide synthase, myoglobin, and myeloperoxidase (*46*−*48*). This radical has further been implicated in the oxidation of organic substrates by myoglobin and H_2O_2 (*49*).

Lipid Peroxidation Is not Critical to Enzyme Inactivation. Although AAPH produces water soluble free radical species, primarily targeting the cytoplasmic domains of the SR Ca^{2+}-ATPase, AAPH has also been shown to stimulate peroxidation of vesicular membrane lipids, suggesting that functionally important transmembrane domains of the Ca^{2+}-ATPase could be damaged by lipid peroxyl radicals and other products of lipid peroxidation (e.g., hydroxynonenal and malondialdehyde) (*14*, *50*, *51*). However, we note only a small degree of peroxidation in SR lipids under the experimental conditions employed in this work and that neither the time course of malondialdehyde production nor the total extent of lipid peroxidation correlates with enzyme inactivation (Figure 7C). Thus we have focused on the resolution of oxidative modifications within the cytoplasmic (extramembranous) domain of the Ca^{2+}-ATPase (*52*).

From the separation of tryptic peptides we identified six distinct peptides of the Ca^{2+}-ATPase: (i) Glu_{121} to Lys_{128}, (ii) His_{190} to Lys_{218}, (iii) Asn_{330} to Lys_{352}, (iv) Gly_{432} to Lys_{436}, (v) Glu_{551} to Arg_{604}, and (vi) Glu_{657} to Arg_{671}, which showed a general oxidative sensitivity to both AAPH-derived radical species and hydrogen peroxide. We also document amino acid residues, e.g., Lys, Arg, His, Met, Thr, Tyr, Cys, and Trp, which are sensitive to AAPH-stimulated oxidation of the SR Ca^{2+}-ATPase. These modified residues may represent more solvent-exposed and chemically reactive side chains within the three-dimensional structure of the Ca^{2+}-ATPase. In other cases direct modification of a sequence is not observed; rather, it has an altered conformation probably resulting from chemical modification of a nearby sequence. Although these peptides are generally sensitive to modification by AAPH-derived radicals and hydrogen peroxide, another reactive oxygen species, peroxynitrite, exhibits quite different effects on the Ca^{2+}-ATPase (*17*). For example, Ca^{2+}-ATPase cysteines are most susceptible to oxidation by peroxynitrite with concomitant formation of intermolecular disulfides. Oxidation of small amounts of Met, Lys, Phe, Thr, Ser, Leu, and Tyr comprise only secondary effects. Thus, in cases of physiological oxidative stress, specific modifications of a marker protein, such as the Ca^{2+}-ATPase, may provide clues to the mechanism of radical-induced cellular damage. Previous studies have also shown that cross-linking or fragmentation of polypeptide chains may be generally induced by free radicals (*53*, *54*). In the study

described here, as well as in a previous study, we find that the SR Ca^{2+}-ATPase is susceptible to protein aggregation but not to fragmentation under conditions of oxidative stress (*17*). The sensitivity of the Ca^{2+}-ATPase to aggregation may result, in part, from its high degree of packing density within the SR membrane with the precise mechanism of cross-linking depending upon the particular reactive oxygen species involved.

ACKNOWLEDGMENT

We thank Robert Drake and Homigol Biesiada for their efforts in acquiring the FAB spectra. A.G.K. was a Post-doctoral Fellow of the Marion Merrell Dow Foundation during the course of this work.

REFERENCES

1. Slater, T. F. (1984) *Biochem. J. 222*, 1−13.
2. Halliwell, B., and Gutteridge, J. M. C., Eds. (1989) *Free Radicals in Biology and Medicine*, 2nd ed., Oxford University Press, New York.
3. Kukreja, R. C., and Hess, M. L. (1994) *Free Radicals, Cardiovascular Dysfunction, and Protection Strategies*, R. G. Landes Co., Austin, TX.
4. Chance, B., Sies, H., and Boveris, A. (1979) *Physiol. Rev. 59*, 527−605.
5. Pryor, W. A., Hales, B. J., Premovic, P. I., and Church, D. F. (1983) *Science 220*, 425−427.
6. Nicotera, P., Kass, G. E. N., Duddy, S. K., and Orrenius, S. (1991) in *Calcium, Oxygen Radicals, and Cellular Damage* (Duncan, C. J., Ed.) pp 17 −35, Cambridge University Press, Cambridge.
7. Kukreja, R. C., and Hess, M. L. (1992) *Cardivasc. Res. 26*, 641−655.
8. Gafni, A., and Yuh, K. M. (1989) *Mech. Ageing Dev. 49*, 105−117.
9. Ferrington, D. A., Jones, T., Squier, T., and Bigelow, D. (1993) *Biophys. J. 65*, A305.
10. Viner, R. I., Ferrington, D. A., Hühmer, A. F. R., Bigelow, D. J., and Schöneich, C. (1996) *FEBS Lett. 379*, 286−290.
11. Barclay, L. R. C., Locke, S. J., MacNeil, J. M., Vankessel, J., Burton, G. W., and Ingold, K. U. (1984) *J. Am. Chem. Soc. 106*, 2479−2481.
12. Niki, E. (1990) *Methods Enzymol. 186*, 100−107.
13. Dean, R. T., Hunt, J. V., Grant, A. J., Yamamoto, Y., and Niki, E. (1991) *Free Radical Biol. Med. 11*, 161−168.
14. Krainev, A. G., and Bigelow, D. J. (1996) *J. Chem. Soc., Perkin Trans. 2, 4*, 747−754.
15. Krainev, A. G., Williams, T. D., and Bigelow, D. J. (1996) *J. Magn. Reson. B 111*, 272 −280.
16. Stadtman, E. R. (1993) *Annu. Rev. Biochem. 62*, 797−821.
17. Viner, R. I., Hühmer, A. F. R., Bigelow, D. J., and Schöneich, C. (1996) *Free Radical Res. 24* (4), 243−259.
18. Fernandez, J. L., Rosemblatt, M., and Hidalgo, C. (1980) *Biochim. Biophys. Acta 599*, 552−568.
19. Warren, G. B., Toon, P. A., Birdsall, N. J. M., Lee, A. G., and Metcalfe, J. C. (1974) *Proc. Natl. Acad. Sci. U.S.A. 71*, 622−626.
20. Lowry, O. H., Rosebrough, N. Y., Farr, A. L., and Randall, R. J. (1951) *J. Biol. Chem. 193*, 266−275.
21. Gornal, A., Bardawill, C., and David, M. (1949) *J. Biol. Chem. 177*, 751−766.
22. Lanzetta, P. A., Alvarez, L. J., Reinsen, P. S., and Candia, O. A. (1979) *Anal. Biochem. 100*, 95−97.
23. Weber, R., and Osborne, J. (1969) *J. Biol. Chem. 244*, 4406−4412.
24. Laemmli, U. K. (1970) *Nature 227*, 680−685.
25. Ellman G. L. (1959) *Arch. Biochem. Biophys. 82*, 70−77.
26. Ritov, V. B., Goldman, R., Stoyanovsky, D. A., Menshikova, E. V., and Kagan, V. E. (1995) *Arch. Biochem. Biophys. 321*, 140−152.
27. Verweij, H., Christianse, K., and van Steveninck, J. (1982) *Biochim. Biophys. Acta 701*, 180−184.
28. Cordis, G. A., Maulik, N., Bagchi, D., Engelman, R. M., and Das, D. K. (1993) *J. Chromatogr. 632*, 97−103.
29. Rupley, J. A. (1967) *Methods Enzymol. 11*, 905−917.
30. Bishop, J. E., Squier, T. C., Bigelow, D. J., and Inesi, G. (1988) *Biochemistry 27*, 5233−5240.
31. Kassel, D. B., Williams, K. P., Musselman, B. D., and Smith, J. A. (1991) *Anal. Chem. 63*, 1978−1983.
32. Malencik, D. A., and Anderson, S. R. (1991) *Biochem. Biophys. Res. Commun. 178*, 60−67.
33. Gaskell, S. J., Reily, M. H., and Porter, C. J. (1988) *Rapid Commun. Mass Spectrom. 2*, 142−145.
34. Fry, S. C. (1982) *Biochem. J. 204*, 449−455.
35. Roepstorff, P., and Fohlman, J. (1984) *Biomed. Mass Spectrom. 11*, 601.
36. MacLennan, D. H., Brandl, C. J., Korszak, B., and Green, N. M. (1985) *Nature 316*, 696−700.
37. Thorley-Lawson, D. A., and Green, N. M. (1977) *Biochem. J. 167*, 739−748.
38. Esterbauer, H., and Jürgens, G. (1993) *Curr. Opin. Lipidol. 4*, 114−124.
39. Green, N. M., Taylor, W. R., Brandl, C. J., Korszak, B., and MacLennan, D. H. (1985) *CIBA Found. Symp. 122*, 93−114.
40. Bigelow, D. J., Squier, T. C., and Thomas, D. D. (1986) *Biochemistry 25*, 194−202.
41. Bigelow, D. J., and Thomas, D. D. (1987) *J. Biol. Chem. 262*, 13449−13456.
42. Squier, T. C., Hughes, S. E., and Thomas, D. D. (1988) *J. Biol. Chem. 263*, 9162−9170.
43. Birmachu, W., and Thomas, D. D. (1990) *Biochemistry 29*, 3904−3914.
44. Farber, J. M., and Levine, R. L. (1986) *J. Biol. Chem. 261*, 4574−4578.
45. Neužil, J., Gebicki, J. M., and Stocker R. (1993) *Biochem. J. 293*, 601−606.
46. Smith, W. L., Eling, T. E., Kulmacz, R. J., Marnett, L. J., and Tsai, A. (1992) *Biochemistry 31*, 3−7.
47. Ortiz de Montellano, P. R., and Catalano, G. E. (1985) *J. Biol. Chem. 260*, 9265−9271.
48. Savenkova, M. I., Mueller, D. M., and Heinecke, J. W. (1994) *J. Biol. Chem. 269*, 20394−20400.
49. Butler, J., Land, E. J., Prütz, W. A., and Swallow, A. J. (1982) *Biochim. Biophys. Acta 705*, 150−162.
50. Palozza, P., Moualla, S., and Krinsky, N. I. (1992) *Free Radical Biol. Med. 13*, 127−136.
51. Sato, Y., Kamo, S., Takahashi, T., and Suzuki, Y. (1995) *Biochemistry 34*, 8940−8949.
52. MacLennan, D. H. (1990) *Biophys. J. 58*, 1355−1365.
53. Huang, W.-H., Wang, Y., and Askari, A. (1992) *Int. J. Biochem. 24*, 621−626.
54. Guptasarma, P., Balasubramanian, D., Matsugo, S., and Saito, I. (1992) *Biochemistry 31*, 4296−4303.
55. Murphy, A. (1976) *Biochemistry 15*, 4492−4496.
56. Brandl, C. J., Green, N. M., Korczak, B., and MacLennan, D. H. (1986) *Cell 44*, 597−607.
57. Kikugawa, K., Kato, T., and Okamoto, Y. (1994) *Free Radical Biol. Med. 16*, 373−382.

BI970058Z